Chapter 4

# Fluorinated Porphyrinic Crystalline Solids: Structural Elucidation and Study of Intermolecular Interactions

Subramaniam Sujatha and Chellaiah Arunkumar

Additional information is available at the end of the chapter

http://dx.doi.org/10.5772/62946

**Abstract**

Crystal engineering is an emerging area of research in material, biological, and pharmaceutical chemistry that involves synthesis of new materials, analysis of its structure including intermolecular interactions using X-ray crystallography as well as computational methods. It has been shown that the intermolecular interactions involving organic fluorine such as C–F•••H, F•••F, and C–F•••π play an important role in stabilizing the supramolecular assemblies, especially in the absence of strong intermolecular forces. Recently, non-covalent interactions involving conjugated aromatic system such as porphyrins have been studied intensively. The synthetic porphyrins are of widespread attention because of their close resemblance to naturally occurring tetrapyrrolic pigments and they find various materials and biological applications. In this book chapter, we disclose our recent findings on detailed crystal structure analysis of a few series of fluorinated porphyrins using single-crystal XRD as well as computational Hirshfeld surface analysis to understand the role of close contacts involving fluorine in the molecular crystal packing.

**Keywords:** Porphyrinoids, fluorinated porphyrins, crystal structure elucidation, intermolecular interactions, Hirshfeld surfaces

## 1. Introduction

Porphyrins are highly conjugated tetrapyrrolic pigments widely found in nature. They play a significant role in biological functions such as electron transfer, oxygen transport, and photosynthetic processes [1]. Most of the naturally occurring macro molecules such as hemoglobin chlorophyll, cytochromes have porphyrin as the basic unit. In these large classes of intensely colored macrocyclic pigments, the four pyrrole subunits are interconnected by methine bridges.

The synthesis of porphyrins can be achieved using the synthetic routes namely Rothemund method, Adler-Longo method, or Lindsey method [2–6]. Synthetic porphyrins are of two types, which include $\beta$-substituted and *meso*-substituted porphyrins. The structure of $\beta$-substituted porphyrins shows close resemblance to naturally occurring porphyrins, whereas the *meso*-substituted porphyrins display potential applications such as biomimetic photosynthesis, molecular electronics, supramolecular catalysis, and organic synthesis [7, 8]. Due to their promising photophysical properties, such as long wavelength absorption and emission, easy functionalization, high singlet oxygen quantum yield and low in vivo toxicity, they also found employed in magnetic resonance imaging (MRI) and photodynamic therapy (PDT) [9–11]. They are the fascinating molecules because of their distinct structure of altering the central metal atom, high thermal stability, tunable shape, symmetry, and synthetic versatility for their physico-chemical properties [8]. The position of the functional groups on the porphyrin building blocks alter the molecular packing and hence their supramolecular assemblies.

In recent years, fluorinated porphyrins are shown much attention since the pharmacological properties can be enhanced by the incorporation of fluorine atoms, and they are very effective in bio-medical applications [12, 13]. The reason behind the fact is that the little atom fluorine is having unique properties such as metabolic stability, binding selectivity, absorption, distribution, and excretion characteristics. Owing to the high electronegativity with its small size makes fluorine an ideal candidate for the replacement of hydrogen. Importantly, by increasing the lipophilicity and also by reducing the charges present in the molecule, fluorinated drugs possess excellent membrane penetration capability compared to its non-fluorinated counter parts [14]. The fluorinated drugs are numerous, and hence, the study of weak intermolecular interactions involving fluorine is essential in the field of medicinal chemistry to promote the discovery of new drugs of desirable profiles.

Intermolecular interactions are mainly of two categories [15], namely isotropic or directional (C•••C, C•••H, H•••H interactions) that define the size, shape as well as close packing and anisotropic or non-directional (hydrogen bonds, charge transfer interactions, halogen interaction, and heteroatom interactions). The weak individual intermolecular interactions act co-operatively and provide a better stability to the crystal packing. The analysis of nature and strength of intermolecular interactions is really important in the area of crystal engineering in order to design new materials especially drugs of desirable properties. They can be studied using X-ray crystallography as well as computational methods [16]. Interactions involving fluorine are of mainly three kinds, namely C–F•••H, F•••F, and C–F•••$\pi$ which provides stability to form molecular self-assemblies especially in the absence of strong intermolecular forces.

Study of weak interactions involving porphyrins offers an interesting field of research in crystal engineering [17]. The energetically weak interactions such as van der Waals forces, hydrogen bonding, or metal coordination are the holding forces to make the self-assembly of porphyrins and quantifying these non-covalent interactions often brings a better understanding in these supramolecular self-assemblies. In this context, Hirshfeld surface (HS) analysis [18] is an important technique that helps to get the detailed information about the crystal structures in terms of intermolecular interactions. HSs and 2D fingerprint plots (FPs) were

http://dx.doi.org/10.5772/62946

generated using the single crystal X-ray diffraction data by Crystal Explorer 3.1 [19]. The term $d_{norm}$ is a ratio of the distances of any surface point to the nearest interior ($d_i$) and exterior ($d_e$) atom and the van der Waals radii of the atoms [20]. The red color in the HSs indicates the closest contact bearing a negative value of $d_{norm}$ with $d_i + d_e$ is shorter than the sum of the relevant van der Waals radii. Whereas the white color denotes the intermolecular distances close to van der Waals contacts with $d_{norm}$ equal to zero. The contacts longer than the sum of van der Waals radii with positive $d_{norm}$ values are blue in color. The 2D FP ($d_i$ versus $d_e$) recognizes the presence of various non-covalent interactions present in the molecular crystals [21]. In this book chapter, we wish to discuss our recent observations on the detailed crystal structure analysis of a few series of fluorinated porphyrins (**Figure 1**) using single crystal X-ray crystallography. The role of weak intermolecular interactions in the molecular crystal packing was quantitatively analyzed using computational HS analysis by Crystal Explorer 3.1. Also, the role of organic fluorine towards crystal packing is discussed in detail.

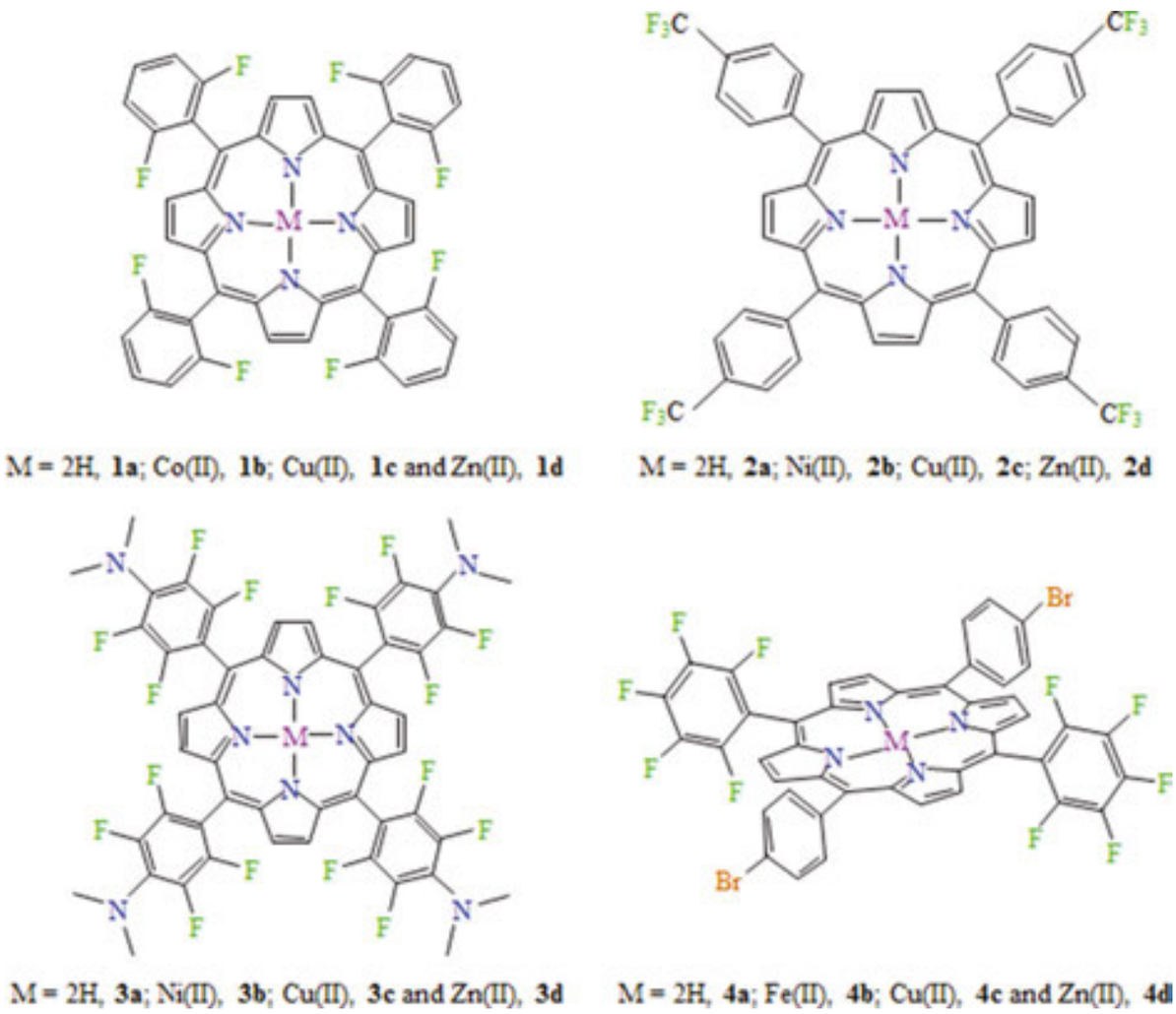


**Figure 1.** Chemical structures of fluorinated porphyrinic crystalline solids under study.

## 2. Synthesis of fluorinated porphyrins

Synthesis of 5,10,15,20-tetrakis(2′,6′-difluorophenyl)porphyrin, $H_2T(2',6'\text{-DFP})P$, **1a** and 5,10,15,20-tetrakis-(4′-trifluoromethylphenyl)porphyrin, $H_2T(4'\text{-}CF_3P)P$, **2a**, were achieved by the treatment of pyrrole with 2,6-difluorobenzaldehyde/4-trifluoromethylbenzaldehyde using the method reported by Lindsey et al. [6]. The porphyrin, $H_2TF_4DMAP$ (5,10,15,20-tetrakis(2′, 3′,5′,6′-tetrafluoro-*N*,*N*-dimethyl-4-anilinyl)porphyrin), **3a** was prepared using $H_2TF_5PP$ (5,10,15,20-tetrakis(pentafluorophenyl)porphyrin) and dimethylamine hydrochloride in DMF at 180 °C under $N_2$ atmosphere using the modified procedure in 85% yield. Consuming 5-(pentafluorophenyl)dipyrromethane and 4-bromobenzaldehyde, the desired *trans*-porphyrin, 5,15-di(pentafluorophenyl)-10,20-bis(4′-bromophenyl)porphyrin was synthesized using the modified procedure of Lindsey et al. [22]. The metal complexes (**1b–1d**, **2b–2d**, **3b–3d,** and **4b–4d**) were prepared by the literature method [23] to afford the desired complexes in quantitative yields. The zinc(II) and copper(II) complexes were obtained in chloroform/methanol mixture using the corresponding metal acetates as metal ion carrier, whereas iron(II), cobalt(II), and nickel(II) complexes were prepared in DMF using metal chloride. All the synthesized porphyrins were isolated, purified by column chromatography and characterized by the conventional spectroscopic methods involving UV-Visible, $^1$H NMR, mass spectrometry, and single-crystal X-ray diffraction analysis.

## 3. Structural determination of fluorinated porphyrins

The single crystals of the porphyrins were grown at room temperature by vapor diffusion method using appropriate solvents. The X-ray data were obtained using a Bruker AXS Kappa Apex II CCD diffractometer with graphite monochromated Mo K$\alpha$ radiation ($\lambda = 0.71073$ Å) at room temperature. The structure solution was done using SIR92 [24] (WINGX32) program by direct methods, and the refinement (full-matrix least squares) was performed on $|F|^2$ using the SHELXL97 [25] software by successive Fourier synthesis with $I > 2\sigma(I)$ reflections.

### 3.1. Structural description of MT(2′,6′-DFP)P (1a–1d)

The porphyrin ligand **1a** containing difluorophenyl group and their metal complexes (**1b–1d**) are crystallized in monoclinic system with half a molecule in the asymmetric unit with space groups $P2_1/c$, $P2_1/n$, $P2_1/c$, and $P2_1/n$ $C2/c$, respectively (**Table 1**). The ORTEP and crystal packing diagrams of **1b–1d** are shown in **Figure 2**. The compounds **1a**, **1c,** and **1b**, **1d** are isostructural with similar crystal packing pattern and the former pair crystallized without solvent molecules in the crystal lattice. The porphyrin plane of **1a** is not ideally planar with maximum deviation of 0.081(1) Å from the mean plane for N2 atom alone. The two difluorophenyl moieties, "C11–C16" and "C17–C22" are inclined to each other through a dihedral angle of 82.71°(6) and 65.85°(5). The distance of 2.686 Å from the centroid of the ring (N2•C6•C7•C8•C9) to H19 #1 is connected by c-glide (*Symm #1.* x, ½−y, -½+z) through C −H•••$\pi$ interactions. Moreover, a 2D sheet of zigzag motifs of molecules formed through C −H•••F (C20−H20•••F3) and C−H•••$\pi$ interactions. These 2D sheets are linked to produce

http://dx.doi.org/10.5772/62946

the 3D network arrangement which is stabilized by the C–H•••F (C15–H15•••F1) interaction. The tetra coordinated copper atom in **1c** lies in the porphyrin core and exhibits perfect square planar geometry with N1–Cu1–N2 bit angle of 90° which makes the porphyrin moiety more planar than the free ligand, **1a**. The porphyrin macrocycle of **1b** is close to planar, the cobalt(II) ion exhibit octahedral geometry and the two methanol molecules coordinated at the apex position. The Co–N distances are equal and in agreement with the reported values [26]. The hydrogen of the coordinated methanol forms O–H•••π interactions with the phenyl ring "C17–C22", the shortest interaction distance of 2.485 (5) Å is given by O1–H1•••C19 #1 contact (Symm: #1 ½–x, ½+y, ½–z). In **1d**, the porphyrin core is planar and the zinc(II) ion is hexa-coordinated and stays in the plane of porphyrin moiety. The average Zn–N and Zn–O distances are 2.054(5) Å and 2.324(5) respectively which is well comparable with that of reported $ZnTPP(THF)_2$ complex [27].

There are no direct π–π and intramolecular interactions seen from the geometrical analysis on the crystal structures of porphyrins, **1a**–**1d**. But, the non-covalent interactions like, $_{(ph,sol)}$C–H•••F, C–H•••$\pi_{(ph,pyr)}$, O–H•••$\pi_{(ph,pyr)}$, C–F•••$\pi_{(ph,sol)}$, and C–H•••O are present in the molecular crystal packing. In addition to these, C–H•••N and F•••F interactions were also present in **1a** and **1b**, **1d,** respectively. The F•••F contact distance in **1b** and **1d** is found to be 2.901 and 2.782 Å, respectively. The crystal structures of **1a** and **1c** mainly contains three types of interactions in the crystal packing such as $_{(ph)}$C–H•••F, C–H•••$\pi_{(pyr)}$, C–F•••$\pi_{(ph)}$, and their distances are in the range of 2.471–2.652 Å, 2.760–2.766 Å and 3.063–3.165 Å, respectively. While in **1b** and **1d**, the types are $_{(ph,sol)}$C–H•••F, C–H•••$\pi_{(ph,pyr)}$, O–H•••$\pi_{(ph,pyr)}$, F•••F, and C–H•••O interactions.

| | **1a** | **1b** | **1c** | **1d** |
|---|---|---|---|---|
| Empirical formula | $C_{44}H_{22}F_8N_4$ | $C_{46}H_{28}CoF_8N_4O_2$ | $C_{44}H_{20}CuF_8N_4$ | $C_{46}H_{28}ZnF_8N_4O_2$ |
| Fw | 758.66 | 879.65 | 820.18 | 886.09 |
| Color | Purple | Pink | Red | Red |
| Crystal system | Monoclinic | Monoclinic | Monoclinic | Monoclinic |
| Space group | P21/c | P21/n | P21/c | P21/n |
| a, Å | 12.5342(10) | 12.426(5) | 12.5477(7) | 12.4217(18) |
| b, Å | 11.4384(9) | 12.723(5) | 11.3955(6) | 12.529(2) |
| c, Å | 12.1720(10) | 12.709(5) | 12.1642(7) | 12.6954(18) |
| α, (°) | 90.0 | 90.000(5) | 90.0 | 90.0 |
| β, (°) | 97.080(3) | 114.615(5) | 96.391 | 114.092(17) |
| γ, (°) | 90.0 | 90.000(5) | 90.0 | 90.0 |
| vol ($Å^3$) | 1731.8(2) | 1826.7(13) | 1728.52(17) | 1803.7(5) |
| Z | 2 | 2 | 2 | 2 |

| | 1a | 1b | 1c | 1d |
|---|---|---|---|---|
| $D_{calcd}$ (mg/m$^3$) | 1.455 | 1.599 | 1.576 | 1.632 |
| Wavelength ($\lambda$), Å | 0.71073 | 0.71073 | 0.71073 | 0.71073 |
| T (K) | 293(2) | 293(2) | 293(2) | 293(2) |
| No. of unique reflections | 2690 | 3583 | 5329 | 3165 |
| No. of parameters refined | 258 | 278 | 259 | 351 |
| GOF on $F^2$ | 1.026 | 1.055 | 1.013 | 1.059 |
| $R_1$[a] | 0.0359 | 0.0488 | 0.0372 | 0.0766 |
| $wR_2$[b] | 0.0818 | 0.1445 | 0.0944 | 0.1685 |

[a]$R_1 = \Sigma||F_o|-|Fc||/\Sigma|F_o|$; $I_o > 2\sigma(I_o)$.

[b]$wR_2 = [\Sigma\, w(F_o^2-F_c^2)^2/\Sigma w(F_o^2)^2]^{1/2}$.

**Table 1.** Crystal structure data of porphyrins under study, **1a**, $H_2$T(2′,6′-DFP)P; **1b**, CoT(2′,6′-DFP)P. 2(MeOH); **1c**, CuT(2′,6′-DFP)P; **1d**, ZnT(2′,6′-DFP)P. 2(MeOH).

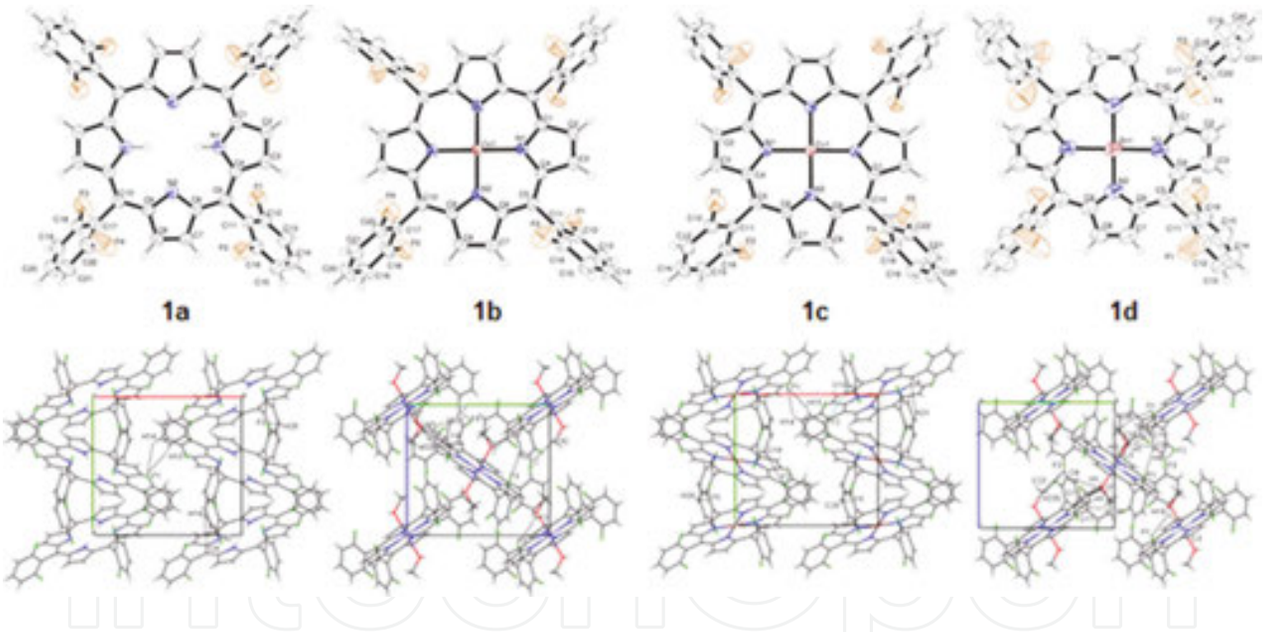


**Figure 2.** ORTEP and molecular crystal packing diagrams of **1a–1d**.

In order to quantify the various intermolecular interactions, HSs and their associated finger print plots were calculated using *Crystal Explorer 3.1*. The HSs of porphyrins, **1a–1d** are illustrated in **Figure 3** showing surfaces that have been mapped with $d_{norm}$. The molecular HSs generated for the two isostructural pairs **1a**, **1c,** and **1b**, **1d** have almost similar shapes reflecting the similar kind of crystal packing modes. The crystal packing of **1b** is mainly controlled by dominant interactions between methanolic OH and phenyl carbon atom whereas in **1d**, be-

http://dx.doi.org/10.5772/62946

tween methanolic OH with pyrrole carbon atom observed as strong red spots. The medium intense red spots are observed for F•••$H_{(ph)}$ contacts in **1a**, **1c** and $_{(pyr)}$H•••$O_{(MeOH)}$ contacts in **1b**, **1d**.

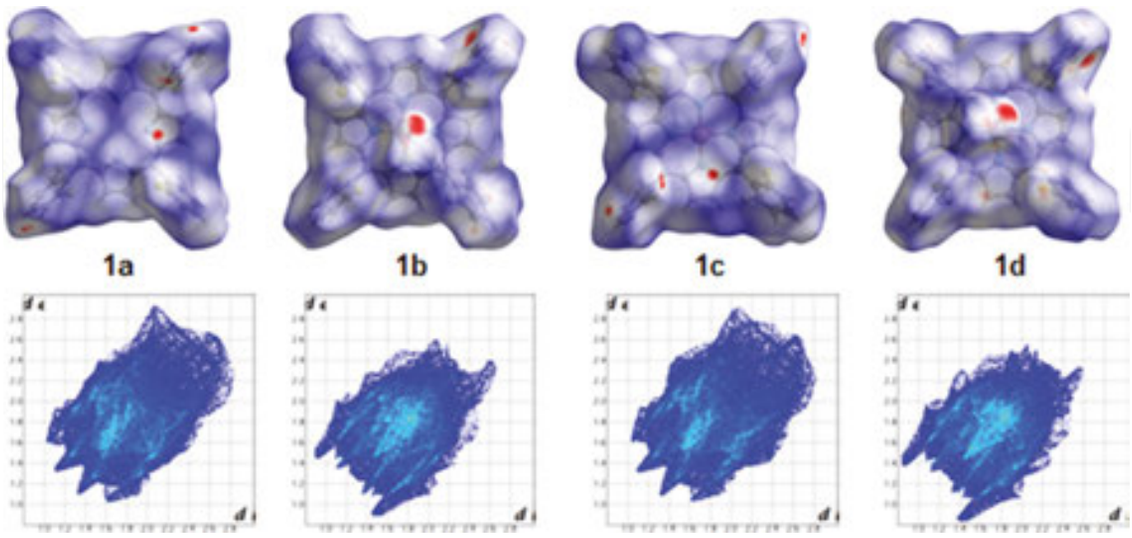


**Figure 3.** Hirshfeld surfaces mapped with $d_{norm}$ ranging from -0.40 Å (red) to 2.50 Å (blue); 2D finger print plots with $d_i$ and $d_e$ ranging from 1.0 to 2.8 Å for **1a–1d.**

From the FP plots, the division of contributions is possible for different interactions including C•••H, F•••H/C/F, H•••H, and N•••H through interactive computer graphics which commonly overlap in the full FP plots. The shapes of FP plots of the two isostructural pairs are comparable The FPs of **1a**–**1d** features spike of various lengths and thickness, and the most prominent being the presence of wing-like peripheral spikes for C•••H contact at the top left and bottom right of each plot and a similar feature is also observed in small organic molecules [18, 28]. In **1a**–**1d**, 26–28% of intermolecular contacts are associated with C•••H and the distance ($d_i + d_e$) is about 2.65 Å for **1a**, **1c** and 2 Å for **1b**, **1d**. The H•••F contact is characterized by a pair of small spikes which also accounts 27–28% of the HSs in **1a**–**1d**. The van der Waals radii of fluorine atom is found to be in the range of 1.35–1.50 Å [29, 30]. The organic fluorine's role in crystal packing of **1a**–**1d** is so prominent because of the F•••H contact distances observed are significantly shorter than the corresponding sum of van der Walls radii (2.45–2.70 Å). The presence of broader spikes (24–34%) for H•••H contacts are in the range of 2.52–2.70 Å [31] which further strengthens the crystal lattice in **1a**–**1d**. The interactions involving fluorine other than H•••F contacts are F•••F (4–6% in **1a**–**1d**), characterized by broad peak; C•••F (7% in **1a**, **1c**; 2% in **1b**, **1d**), characterized by small curved lines/small peaks. The C•••F and F•••F contact distances ($d_i + d_e$) are seen in the range of 3.28–3.48 Å and 2.80–3.02 Å, respectively, which are nearer to the sum of its van der Walls radii (3.03–3.27 Å and 2.70–3.00 Å). Overall, the weak interactions involving fluorine is 35–40%, they can play a crucial role in

directing the supramolecular organization of porphyrins [32]. **Figure 4** shows the distribution of individual intermolecular interactions on the basis of HS analysis for the related compounds.

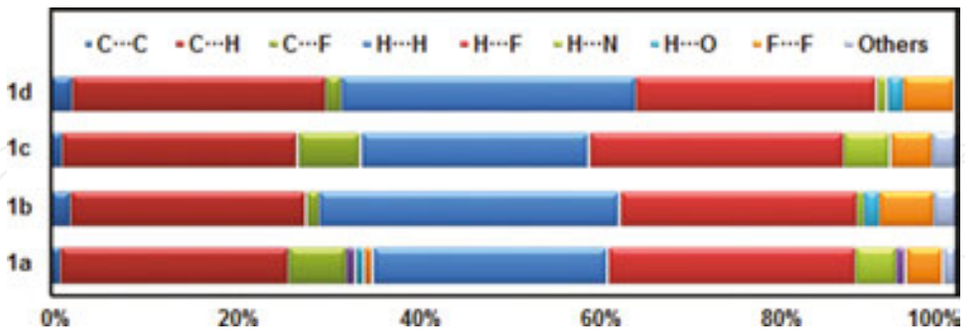


**Figure 4.** Distribution of individual intermolecular interactions on the basis of Hirshfeld surface analysis of **1a–1d.**

### 3.2. Structural description of MT(4′-$CF_3$P)P (2a–2d)

Compounds, **2a** and **2c** were crystallized in triclinic, whereas **2b** and **2d** in monoclinic system (**Table 2**). In all the porphyrins, the solvent molecule THF is either present in the crystalline lattice or they bind to the metal centre which show the well-known envelope conformation as witnessed in the literature [33, 34]. The asymmetric unit of **2a** consists of two half molecules of porphyrins and two THF molecules. The porphyrin core in **2a** exhibit planar skeleton, whereas in **2c,** it is of non-planar, possibly due to the presence of 4-trifuloromethylphenyl groups and an extra THF molecule which makes them being non-isostructural. In compound **2b**, the asymmetric unit contains half molecule of porphyrin and one THF molecule is coordinated to the nickel(II) centre. The ORTEP diagram of **2b** consists nickel(II) ion which is hexa-coordinated with two THF molecules at the apex positions and the molecular crystal packing is formed through C–F•••$H_{(sol)}$ interactions (**Figure 5**). The bond angles N–Ni–$N_{(adj)}$ and N–Ni–$N_{(opp)}$ in **2b** indicates a perfect planar geometry of the porphyrin core.

| | **2a** | **2b** | **2c** | **2d** |
|---|---|---|---|---|
| Empirical formula | $C_{56}H_{42}F_{12}N_4O_2$ | $C_{56}H_{40}F_{12}N_4NiO_2$ | $C_{52}H_{32}CuF_{12}N_4O$ | $C_{52}H_{32}F_{12}N_4OZn$ |
| Fw | 1030.94 | 1087.63 | 1020.36 | 1022.19 |
| CCDC no. | 1013690 | 1013689 | 1011088 | 1011087 |
| Colour | Purple | Violet | Brown | Brown |
| Crystal system | Triclinic | Monoclinic | Triclinic | Monoclinic |
| Space group | P-1 | $P2_1/n$ | P-1 | P21/c |
| a, Å | 11.5014(8) | 14.5791(19) | 9.7136(5) | 19.427(3) |
| b, Å | 13.1179(12) | 9.5303(19) | 14.5452(9) | 9.3940(10) |
| c, Å | 17.3269(15) | 18.351(4) | 16.8870(13) | 25.466(5) |
| a, (°) | 96.329(3) | 90.0 | 76.608(3) | 90.0 |

http://dx.doi.org/10.5772/62946

| | 2a | 2b | 2c | 2d |
|---|---|---|---|---|
| β, (°) | 92.833(3) | 101.571(8) | 89.617(3) | 102.756(5) |
| γ, (°) | 108.739(3) | 90.0 | 76.676(3) | 90.0 |
| Volume (Å$^3$) | 2450.5(4) | 2498.0(8) | 2255.8(3) | 4532.8(12) |
| Z | 2 | 2 | 2 | 4 |
| $D_{calcd}$(mg/m$^3$) | 1.397 | 1.446 | 1.502 | 1.498 |
| λ, Å | 0.71073 | 0.71073 | 0.71073 | 0.71073 |
| T (K) | 173 | 173 | 173 | 173 |
| No. of unique reflections | 8528 | 4413 | 7810 | 7986 |
| No. of parameters refined | 788 | 397 | 825 | 813 |
| GOF on $F^2$ | 1.027 | 1.015 | 1.039 | 1.022 |
| $R_1$[b] | 0.0657 | 0.0477 | 0.0476 | 0.0465 |
| $wR_2$[c] | 0.1849 | 0.1179 | 0.1205 | 0.1129 |

[a]$R_1 = \Sigma||F_o|-|Fc||/\Sigma|F_o|$; $I_o > 2\sigma(I_o)$.

[b]$wR_2 = [\Sigma\, w(F_o^2-F_c^2)^2/\Sigma w(F_o^2)^2]^{1/2}$.

**Table 2.** Crystal structure data of porphyrins under study: 2a, $H_2T(4'\text{-}CF_3P)P.\ (THF)_2$; 2b, $Ni^{II}T(4'\text{-}CF_3P)P.\ (THF)_2$; 2c, $Cu^{II}T(4'\text{-}CF_3P)P.\ (THF)$; 2d, $Zn^{II}T(4'\text{-}CF_3P)P.\ (THF)$.

The copper(II) centre in **2c** is four coordinated with the inner core nitrogens of the porphyrin ring, exhibits non-planarity and the mean plane displacement of the core atoms is ±0.3313 Å

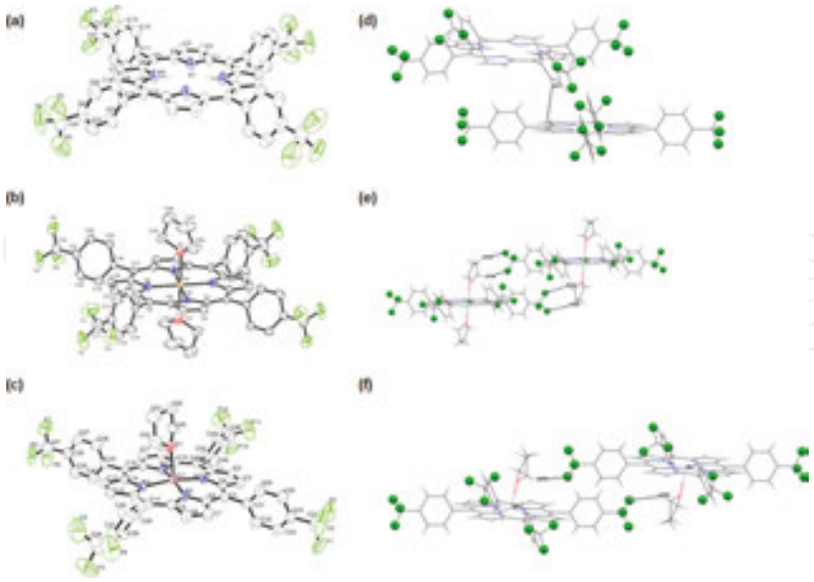


**Figure 5.** ORTEP diagrams and slip-stack orientations of molecules of **2a**, **2b** and **2d** (Solvent molecules and hydrogens are not shown for clarity, thermal ellipsoids are shown at 40% probability level) through C–H•••π; C–F•••$H_{(sol)}$ and C –F•••$H_{(sol)}$ interactions, respectively.

which is less compared to that of the reported $\beta$-pyrrole substituted copper(II) porphyrins [35, 36]. The ORTEP diagrams (top and side view) and packing diagram showing the slip-stack orientation of molecules through C–H•••$\pi$ interactions are also shown in **Figure 6**. The non-planarity of the core is possibly due to 4-trifluoromethylphenyl groups and solvent (THF) molecule present in the lattice.

The zinc(II) centre in **2d** is five coordinated, which exhibits domed shape which is quite known for the zinc(II) complexes and the porphyrin plane is almost planar. However, the nitrogen atoms, N3 and N4 are above the plane with 0.078(3) Å and 0.045(3) Å; N1, N2, and Zn atoms are below the plane with 0.107(3) Å, 0.074(3) Å and 0.218(1) Å, respectively [37]. The bound THF is responsible for the metal to be slightly pulled down from the mean plane.

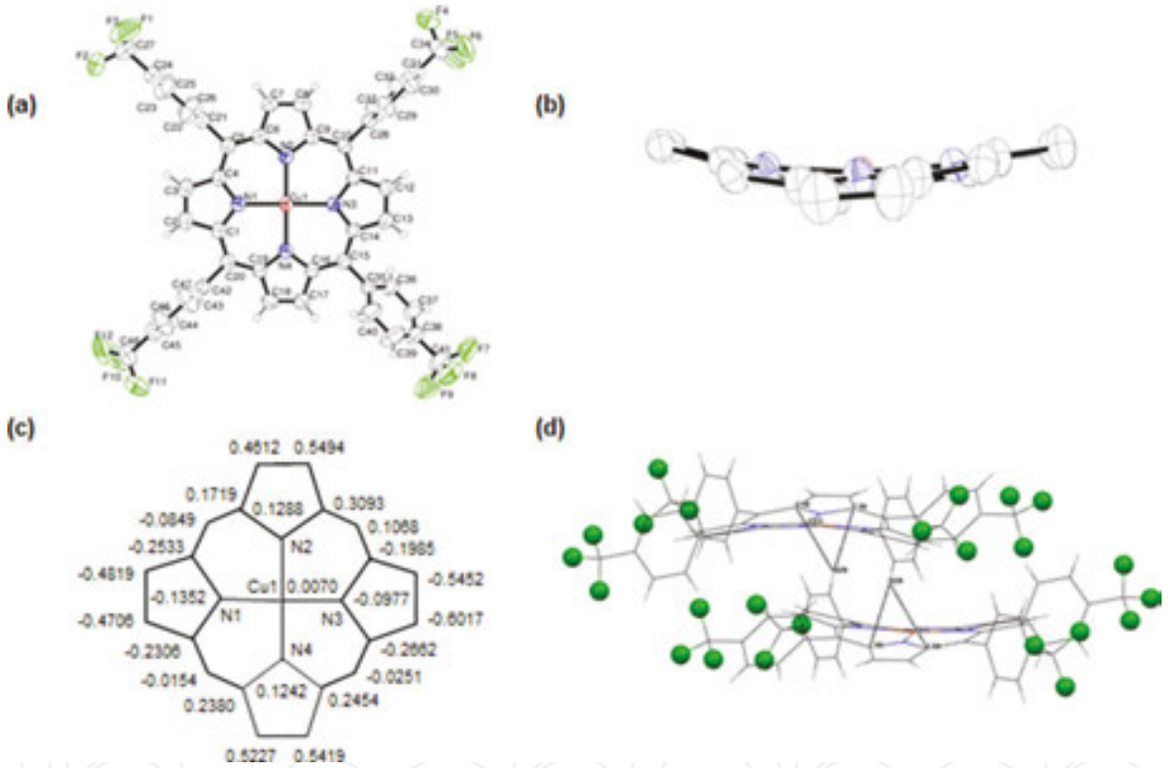


**Figure 6.** ORTEP diagrams of **2c**, (a) top view; (b) side view (solvent molecule is not shown for clarity; thermal ellipsoids are shown at 40% probability level); (c) mean plane displacements of the Cu(II) ion and the core atoms shown in Å units; (d) slip-stack orientation of molecules through C–H•••$\pi$ interactions viewed down 'c' axis.

The geometrical analysis of porphyrins, **2a–2d** reveals that the molecular crystal packing consists of intermolecular interactions viz., $_{(sol/ph/pyr)}$C-H•••F, $_{(sol/ph/pyr)}$C-H•••C$_{(sol/ph/pyr)}$, C-F•••C$_{(ph/pyr)}$, $_{(ph/pyr)}$H•••H$_{(sol)}$, $_{(pyr)}$C–H•••O$_{(sol)}$, and F•••F. Interestingly, the H•••H close contact is seen only in **4** and **5**, and the distance varies from 1.845 to 2.364 Å which is considerably shorter compared with the previously discussed fluorinated porphyrins. The HSs, which have been mapped over a $d_{norm}$ range of -0.14 to 2.0 Å, are illustrated in **Figure 7**.

http://dx.doi.org/10.5772/62946

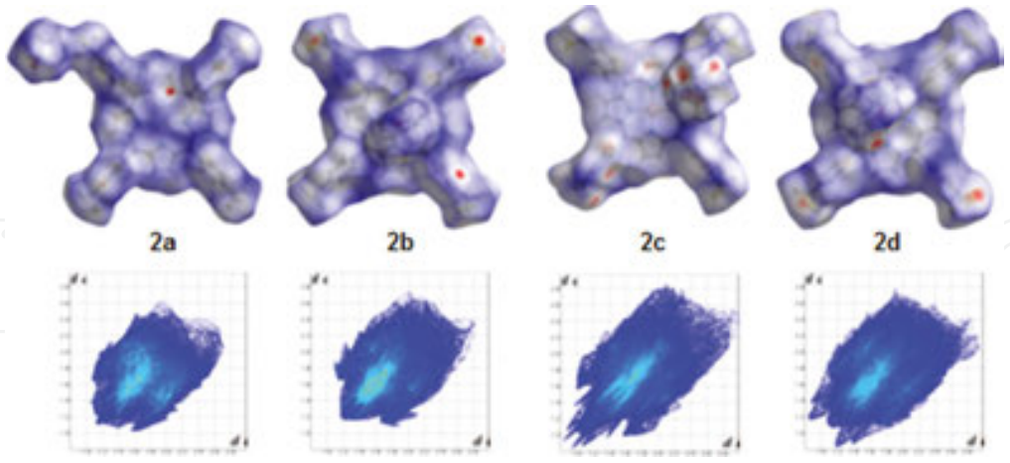


**Figure 7.** Hirshfeld surfaces of porphyrins, **2a–2d** with $d_{norm}$ mapped ranging from -0.14 (blue) to 2.02 (red); 2D FPs for the various intermolecular interactions with $d_i$ and $d_e$ ranging from 2.31 to 2.44 Å.

The crystal packing in porphyrins **2a–2d** is mainly controlled by F•••H interaction that is observed as intense red spots on the HSs. The F•••F contacts are also seen as large intense red spots in **2a–2c**. The F•••C contacts are observed as medium intense red spots in free ligand **1a** and its copper derivative **2c** whereas faint red area in zinc derivative **2d**.

Apart from this, porphyrin **2d** shows faint red spots for N•••F close contact. In addition to the close contacts involving fluorine, C•••H contacts are appeared as intense and/or faint red spots in porphyrins **2a** and **2c** and the red spots are also seen in H•••H contacts of **2a** and **2b.** The shape of the FPs of porphyrins in **2a–2d** is unique indicating that there are no isostructural pair and the most dominant interaction is F•••H contacts seen at the middle region of each plot (**Figure 7**). In **3** and **4**, 44% of intermolecular contacts are associated with F•••H contacts, whereas in **2a** and **2b,** they are associated with 36 and 39% of the HSs respectively. And the distance ($d_i + d_e$) is about 2.31–2.44 Å for **2a–2d** which are significantly shorter than the corresponding sum of van der Walls radii (2.45–2.70 Å) indicating its significant role in crystal packing [29, 30]. The interactions involving fluorine other than F•••H contacts are F•••F and F•••C (4–5%) with $d_i + d_e$ value in the range of 2.59–2.96 Å and 3.14–3.20 Å, respectively. Also, the C•••H contacts are appeared at the top left and bottom right of each plot, and the percentage contributions are 12–18%, respectively, for **2a–2d**. The FPs of H•••H contact are somewhat closer in nature compared to the previously discussed fluorinated porphyrins. Overall, the interactions involving fluorine are 46% for **2a** and 53–55% for **2b–2d**, which plays a major role in directing the supramolecular architecture of porphyrins (**Figure 8**) [38]. Apart from those above, the presence of other contacts such as O•••H, N•••H and N•••F interactions were also observed.

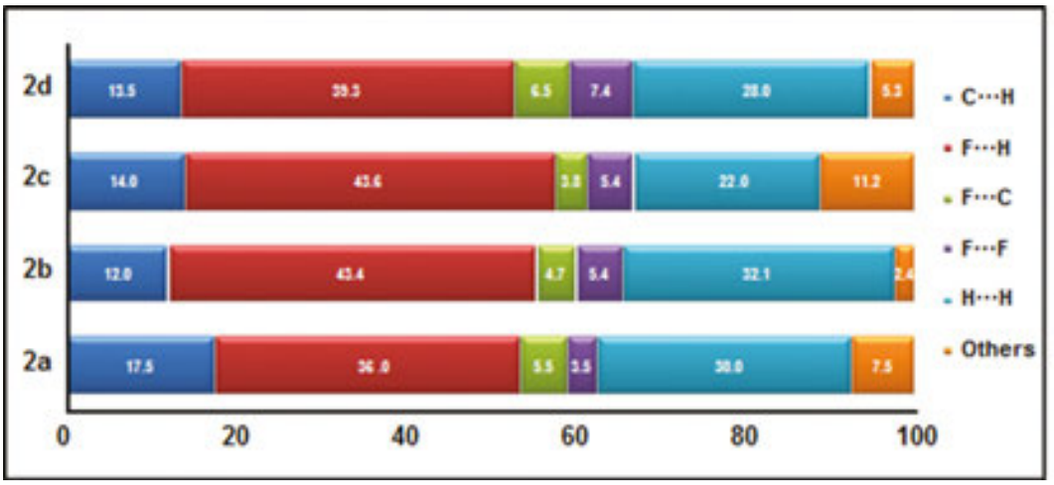


**Figure 8.** Percentage contribution of non-covalent interactions in porphyrins, **2a–2d** on the basis of HSs.

### 3.3. Structural description of $MTF_4DMAP$ (3a–3d)

Porphyrins **3a** and **3c** are isostructural, crystallized in triclinic system (**Table 3**) and the asymmetric unit consists of crystallographically independent two halves of molecules with disordered water molecules in the crystal lattice (**Figure 9**). In **3a**, the porphyrin moiety of both molecules is planar within the limits of standard deviation and the conformation of the two molecules is slightly different. The packing is mostly stabilized through four, fairly strong, intermolecular C–H•••F hydrogen bonds. In **3c**, the copper(II) ion is located at an inversion centre with square planar environment. The Cu–N bond length in equatorial plane varies between 1.976(3) and 1.999(3) Å. The $(N–M–N)_{adj}$ angle is 90° and the $(N–M–N)_{opp}$ angle is 180° indicating the perfect square planar geometry around the Cu(II) metal centre.

| | **3a** | **3b** | **3c** | **3d** |
|---|---|---|---|---|
| Empirical formula | $C_{52}H_{40}F_{16}N_8O_2$ | $C_{60}H_{48}F_{16}N_8NiO_2$ | $C_{52}H_{36}CuF_{16}N_8O_2$ | $C_{64}H_{56}F_{16}N_8O_3Zn$ |
| Fw | 1112.92 | 1275.77 | 1172.43 | 1354.54 |
| Color | Purple | Pink | Red | Purple |
| Crystal system | Triclinic | Tetragonal | Triclinic | Tetragonal |
| Space group | P-1 | $P4_2/n$ | P-1 | I4 |
| a, Å | 10.2706(5) | 15.9979(5) | 10.2273(5) | 16.4305(3) |
| b, Å | 14.6333(7) | 15.9979(5) | 14.6303(6) | 16.4305(3) |
| c, Å | 18.0523(9) | 10.9552(7) | 17.9791(7) | 11.1822(5) |
| α, (°) | 86.258(2) | 90 | 86.664(2) | 90 |
| β, (°) | 86.484(2) | 90 | 86.704(2) | 90 |
| γ, (°) | 74.150(2) | 90 | 74.494(2) | 90 |
| vol ($Å^3$) | 2601.7(2) | 2803.8(2) | 2585.42(19) | 3018.76(16) |

http://dx.doi.org/10.5772/62946

| | 3a | 3b | 3c | 3d |
|---|---|---|---|---|
| Z | 2 | 2 | 2 | 2 |
| $D_{calcd}$ (mg/m$^3$) | 1.421 | 1.511 | 1.506 | 1.490 |
| wavelength ($\lambda$), Å | 0.71073 | 0.71073 | 0.71073 | 0.71073 |
| T (K) | 293(2) | 293(2) | 293(2) | 293(2) |
| No. of unique reflections | 6143 | 2169 | 5964 | 2605 |
| No. of parameters refined | 798 | 197 | 779 | 221 |
| GOF on $F^2$ | 1.111 | 1.075 | 1.103 | 1.077 |
| $R_1$[a] | 0.0640 | 0.0522 | 0.0428 | 0.0410 |
| $wR_2$[b] | 0.1930 | 0.1529 | 0.1151 | 0.1083 |

[a] $R_1 = \Sigma||F_o|-|Fc||/\Sigma|F_o|$; $I_o > 2\sigma(I_o)$.

[b] $wR_2 = [\Sigma w(F_o^2-F_c^2)^2/\Sigma w(F_o^2)^2]^{1/2}$.

**Table 3.** Crystallographic data of porphyrins, 3a–d.

Compound **3b** and **3c** crystallizes in tetragonal system with space group $P4_2/n$ and I4, respectively, and the metal centre is four coordinated. The porphyrin macrocycle in **3b** is non-planar, and there is a fairly strong intermolecular halogen–π interaction given by C3···F2 #1 (*Symm #1: 1–x, 1–y, z*) with distance 2.992(5) Å and another weak halogen–π intermolecular interaction by C10···F1 #1 with distance 3.152(6) Å. The bond angles, $(N–M–N)_{adj}$ and $(N–M–N)_{opp}$ are 90° and 173.0°, respectively, indicating that the Ni(II) centre in **3b** is deviated from square planar geometry. The tetra-coordinated porphyrins, **3b** and **3c** possess the average M–N bond lengths of 1.938(3) Å and 1.989(3) Å, respectively. Porphyrin **3d** is penta-coordinated with a THF molecule and the asymmetric unit consists of one-fourth of the porphyrin molecule solvated with half of the THF molecule in the crystal lattice.

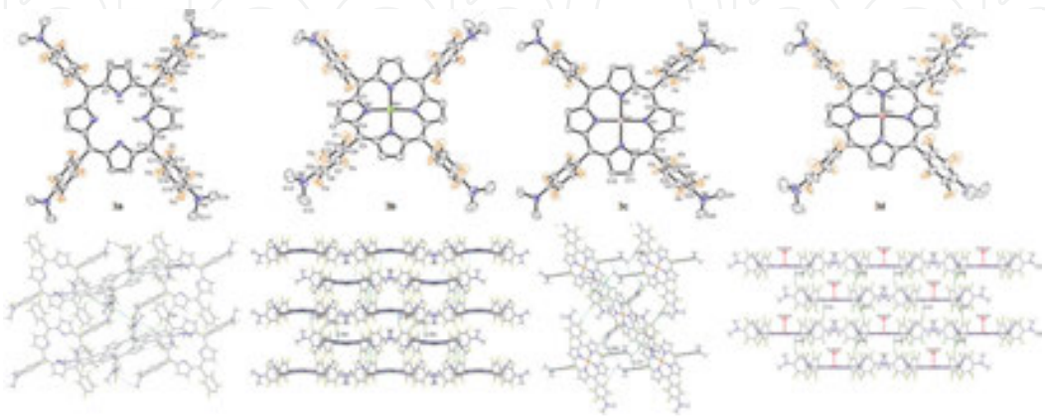

**Figure 9.** ORTEP and molecular crystal packing diagrams of **3a–3d.**

The average Zn–N and Zn–O distance in **3d** is 2.052(3) Å and 2.130(6) Å respectively and the values are in good agreement with that of the reported penta-coordinated Zn(II) complexes [24]. In **3a** and **3c, t**here is a strong C···H interaction involving $C(NMe_2)$–H···$C_{(porp)}$ observed. Apart from these, several other intermolecular interactions involving fluorine such as C–H···F contact in which the fluorine interacts with the hydrogen of the $\beta$−pyrrole ring (2.338–2.799 Å) and C–F···π and F···F interactions are observed.

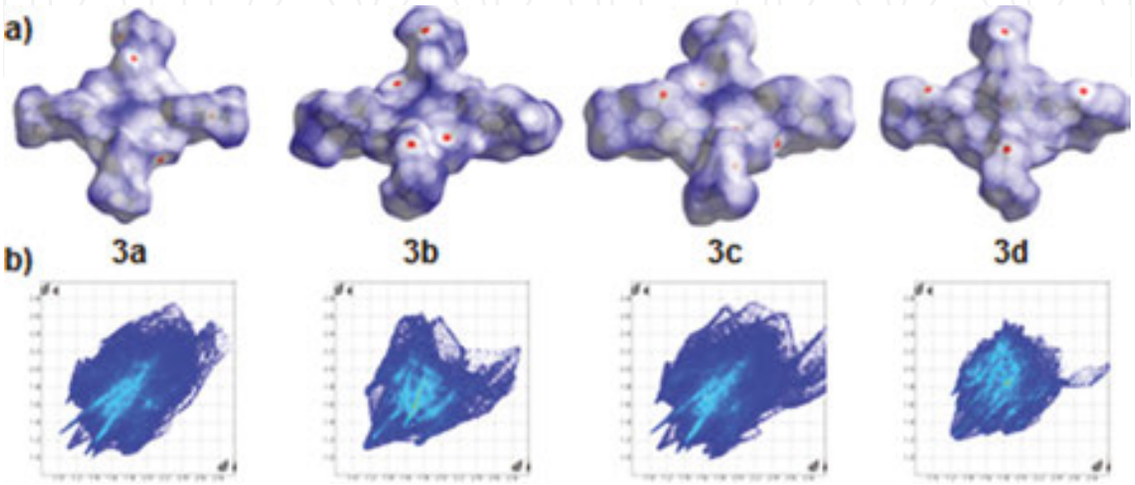


**Figure 10.** Hirshfeld surfaces with normalized contact distance ranging from -0.4 Å (red) to 2.0 Å (blue) and (b) 2D finger print plots of all the intermolecular contacts with $d_i$ and $d_e$ ranging from 1.0 to 2.8 Å for **3a–3d.**

The HSs of molecules **3a** and **3c** have similar shapes indicating similar interactions in the packing modes (**Figure 10**). The presence of the coordinated THF molecule to the Zn(II) is reflected in different size and shape of the HS at the centre of **3d** as compared to the flat surface at the centre of **3a**–**3c**. The crystal packing of **3a** and **3c** is mainly controlled by dominant interactions involving C•••H, F•••H, and F•••F contacts observed as red spots on the HSs whereas in **3b** it is F•••C and in **3d** it is of F•••H contacts. In the isostructural crystals, **3a** and **3c**, 15% of intermolecular contacts are associated with C•••H, whereas in **3b** and **3d** it is 12 and 26% of the HSs and the distance ($d_i + d_e$) is about 2.80 Å for **3a**–**3d**. The interactions involving fluorine are H•••F (43% in **3a**, **3c**; 33% in **3c**; 23% in **3d**); F•••F (6–7% in **3a**–**3d**). The $d_i + d_e$ value observed for H•••F contacts are about 2.40 Å for **3a**, **3c**; 2.70, and 1.85 Å for **3b**, **3d,** respectively, whereas F•••F contacts are in the range of 2.80–3.25 Å. In **3a** and **3c**, the different types of C–F···π interactions has the least contribution towards the total intermolecular interactions (3.0%), and the shortest close-contact distance ($d_i + d_e$) is about 3.2 Å. For the compounds **3b** and **3d**, it is found to be 11 and 16%, respectively, with $d_i + d_e$ is about 3.0 Å. As inferred from the geometrical analysis, the C–F···π interaction is primarily responsible for the crystal packing in **3b** indicated by the red spots in the HS (**Figure 10**). The H•••H contacts are characterized by sharper spikes in **3a**–**3d** (17–30%). **Figure 11** shows the contributions of various types of interactions in the HSs for all the investigated porphyrins. The decomposition of the FPs emphasizes that the weak interactions involving fluorine atom can act as the major

http://dx.doi.org/10.5772/62946

contributors for the crystal packing in addition to the C•••H contacts and the cooperativity of the H•••H contacts [39].

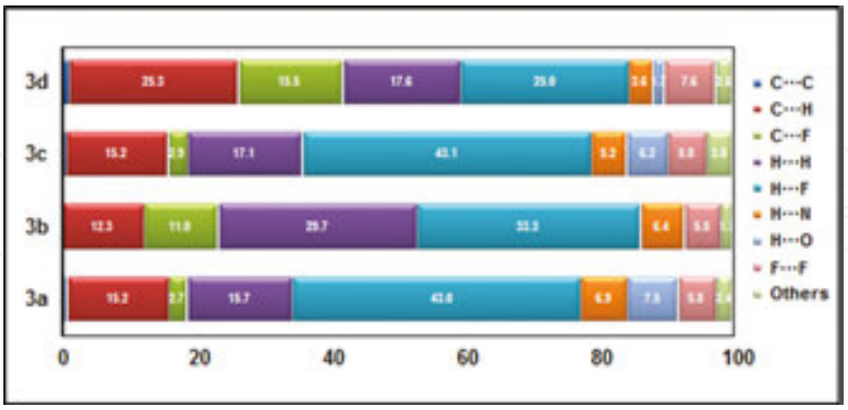


**Figure 11.** Relative percentage contribution of various intermolecular interactions in **3a–3d** based on Hirshfeld surface analysis.

### 3.4. Structural description of 5,15-di(pentafluorophenyl)-10,20-bis(4′-bromophenyl)porphyrin and its metal complexes (4a–4d)

*Trans*-porphyrins, **4a** and **4c** were crystallized in monoclinic with $P2_1/c$ space group whereas **4b** and **4d** in triclinic with P-1 space group (**Table 4**). The free ligand and the Cu(II) complex crystallized without solvent molecules. In **4b,** there are two pyridine molecules present at the apex positions and in **4d,** one of the THF molecule is coordinated to the zinc(II) centre, while another one is seen in the crystal lattice. As seen earlier, the bound or unbound THF solvate molecules in **4d** show the well-known envelope conformation [33, 34]. The asymmetric unit of **4a** and **4c** consists of half molecule of porphyrin in which both porphyrin cores are found to be planar in nature. The copper(II) centre in **4c** is tetra-coordinated with the inner core nitrogen of the porphyrin ring. The ORTEP and packing diagrams of the isostructural **4a** and **4c** are shown in **Figure 12**. The asymmetric unit of **4b** contains two half molecules of porphyrin each bearing a pyridine residue as solvent attached to the iron(II) centre. The iron(II) ion is hexa-coordinated with two pyridine molecules at the apex positions and the molecular crystal packing diagrams of **3** forms a orthogonal arrangements in a one dimensional array of molecules through C•••H and F•••F interactions viewed down 'c' axis. The zinc(II) centre in **4d** is penta-coordinated and exhibits domed shape which is quite common for the zinc(II)-porphyrin complexes. The porphyrin plane with the metal atom is almost planar. However, the atoms N1, N4, and Zn are above the plane with 0.0896(5) Å, 0.1081(5) Å, and 0.1409(1) Å; N2 and N3 atoms are below the plane with 0.3491(5) Å and 0.2406(5) Å, respectively.

Like other fluorinated porphyrins discussed earlier, the crystal packing of trans porphyrins **4a –4d** consists of a number of intermolecular interactions viz., $_{(sol/ph/pyr)}$C-H•••F, $_{(sol/ph/pyr)}$C-H•••Br, $_{(ph)}$C-F•••Br, $_{(sol/ph/pyr)}$C-H•••$C_{(sol/ph/pyr)}$, $_{(ph)}$C-F•••$C_{(ph)}$, $_{(ph/pyr)}$C•••$C_{(sol/ph)}$, $_{(ph/pyr)}$H•••$H_{(sol)}$, $_{(pyr)}$C–H•••$O_{(sol)}$ and F•••F. Interestingly, the symmetrical (F•••F) and unsymmetrical ($_{(ph)}$C-F•••Br) halogen interactions have been identified only in **4a** and **4c**, and the

distance varies from 3.280 to 3.295 Å which is further supported by the HS analysis (**Figure 13**). As anticipated, the free ligand (**4a**) and its copper derivative (**4c**) are isostructural. The HSs mapped with $d_{norm}$ for **4a** and **4c** highlights medium intense red spots for F•••H/F and C•••H close contacts and faint red spots for F•••C/Br contacts. The compound **4b** shows intense red spots for F•••H close contact and faint red spots for H•••Br contact and very pale red spots for F•••H contact, whereas **4d** shows several bright red spots for F•••H, few intense red spots for H•••Br close contact and faint red spots for N/C•••H and C•••F contact. Over all, porphyrin **4d** shows large number of red spots compared to other porphyrins **4a**–**4c** due to the role of lattice as well as coordinated THF molecule toward crystal packing.

| | **4a** | **4b** | **4c** | **4d** |
|---|---|---|---|---|
| Empirical formula | $C_{44}H_{18}Br_2F_{10}N_4$ | $C_{54}H_{26}Br_2F_{10}FeN_6$ | $C_{44}H_{16}Br_2CuF_{10}N_4$ | $C_{52}H_{32}Br_2F_{10}N_4O_2Zn$ |
| Fw | 952.44 | 1164.48 | 1013.97 | 1160.01 |
| CCDC no. | 1013690 | 1013689 | 1011088 | 1011087 |
| Colour | Purple | Red | Purple | Purple |
| Crystal system | Monoclinic | Triclinic | Monoclinic | Triclinic |
| Space group | $P2_1/c$ | P-1 | $P2_1/c$ | P-1 |
| a, Å | 14.9457(6) | 10.700(5) | 14.8461(9) | 12.6848(5) |
| b, Å | 8.9793(4) | 13.933(5) | 8.9921(5) | 13.4661(5) |
| c, Å | 15.9316(6) | 17.329(5) | 15.8111(9) | 16.2952(6) |
| $\alpha$, (°) | 90 | 103.791(5) | 90 | 66.724(2) |
| $\beta$, (°) | 116.550(2) | 100.709(5) | 116.115(3) | 68.750(2) |
| T (K) | 293(2) | 293(2) | 293(2) | 293(2) |
| $\lambda$, Å | 0.71073 | 0.71073 | 0.71073 | 0.71073 |
| $\gamma$, (°) | 90 | 103.144(5) | 90 | 76.468(2) |
| Volume (Å$^3$) | 1912.58(14) | 2363.2(16) | 1895.26(19) | 2369.64(16) |
| Z | 2 | 2 | 2 | 2 |
| $D_{calcd}$ (mg/m$^3$) | 1.654 | 1.636 | 1.777 | 1.626 |
| No. of unique reflections | 3747 | 6952 | 3340 | 8341 |
| No. of parameters refined | 277 | 661 | 277 | 854 |
| GOF on $F^2$ | 1.022 | 1.057 | 1.025 | 1.024 |
| $R_1$[b] | 0.0465 | 0.0551 | 0.0448 | 0.0586 |
| $wR_2$[c] | 0.1317 | 0.1395 | 0.1131 | 0.1468 |

[a]$R_1 = \Sigma||F_o|-|Fc||/\Sigma|F_o|$; $I_o > 2\sigma(I_o)$.

[b]$wR_2 = [\Sigma\, w(F_o^2-F_c^2)^2/\Sigma w(F_o^2)^2]^{1/2}$.

**Table 4.** Crystal structure data of porphyrins under study, MBPFPBBPP; M = 2H, 4a; Fe(II). $(pyridine)_2$, 4b; Cu(II), 4c and Zn(II). $(THF)_2$, 4d.

http://dx.doi.org/10.5772/62946

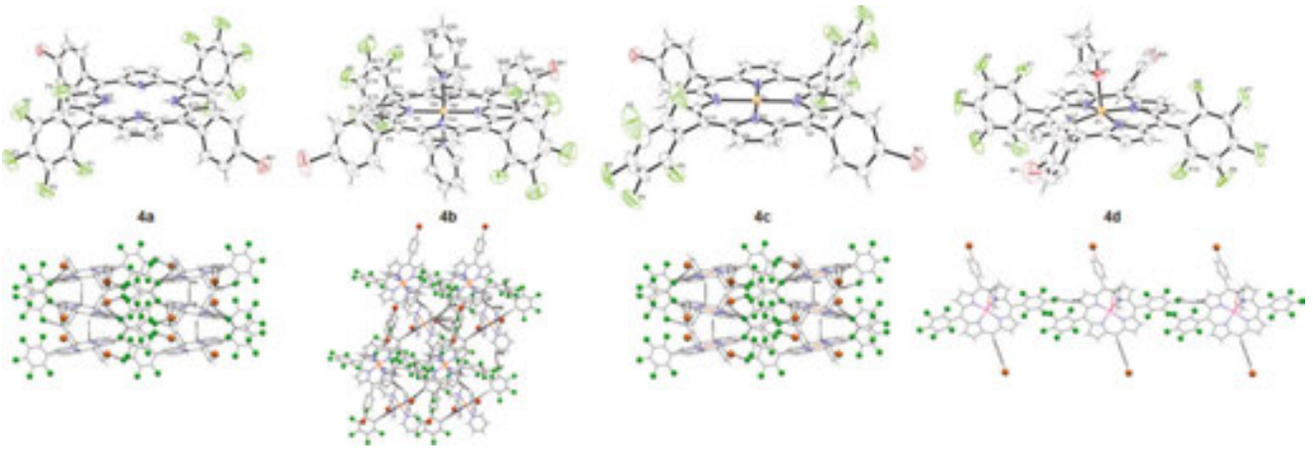


**Figure 12.** ORTEP and molecular crystal packing diagrams of **4a–4d.**

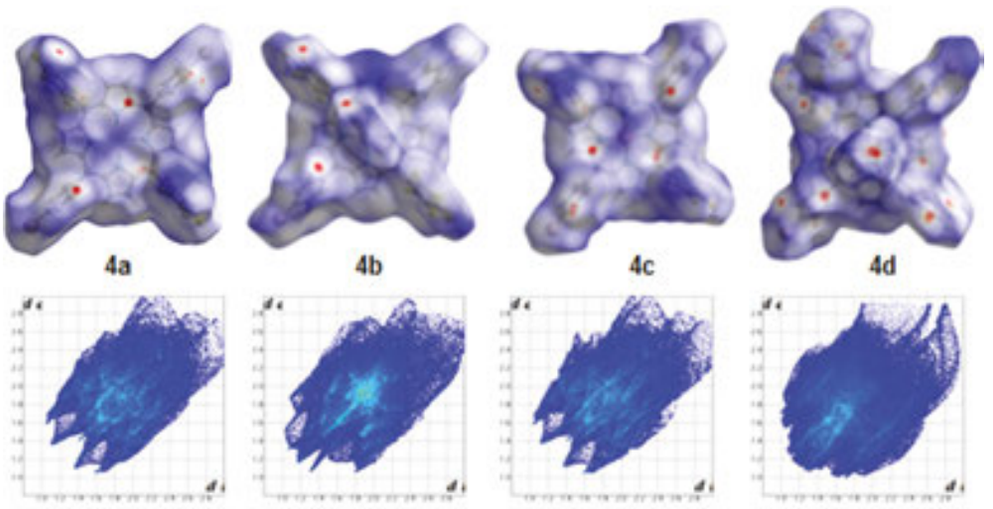


**Figure 13.** Hirshfeld surfaces with $d_{norm}$ mapped ranging from -0.11 (blue) to 1.89 (red) and 2D FPs for the various intermolecular interactions in **4a–4d.**

The prominent spikes in the FP plots of **4a–4d** are associated with close contacts involving halogen atoms (F/Br) and can be attributed to F•••H/F/C, Br•••H/F interactions. It is clear from the analysis that the interactions involving halogens are the major contributors to the total HS area and the relative contributions are 62, 61, 66 and 57%, respectively, for **4a–4d**. Among these, 26–33% of close contacts are associated with F•••H interactions. Both symmetrical F•••F (~2.81 Å) as well as unsymmetrical F•••Br (~3.28 Å) halogen interactions are seen in all porphyrins except that the F•••Br interaction is absent in the case of **4b**. For porphyrins **4b** and **4d**, the F•••F/Br contact distances are broader in nature compared to **4a** and **4c** with no red spots on the HSs. Moreover, there is no F•••Br interaction in the case of iron(II) porphyrin **4b** and none of the porphyrins show Br•••Br interaction.

The C•••H contact is seen as peripheral wing like structure in all the four porphyrins and is associated with 13–18% of the total HSs. The H•••H interactions are more pronounced in iron

and zinc derivative (21–22%), and it contributes only 7–10% for the isostructural pair **4a** and **4c**. The smallest fingerprint contributions occur for N•••H and C•••C. A detailed relative contribution of the different interactions to the HS was of porphyrins **4a–4d** is given in **Figure 14**.

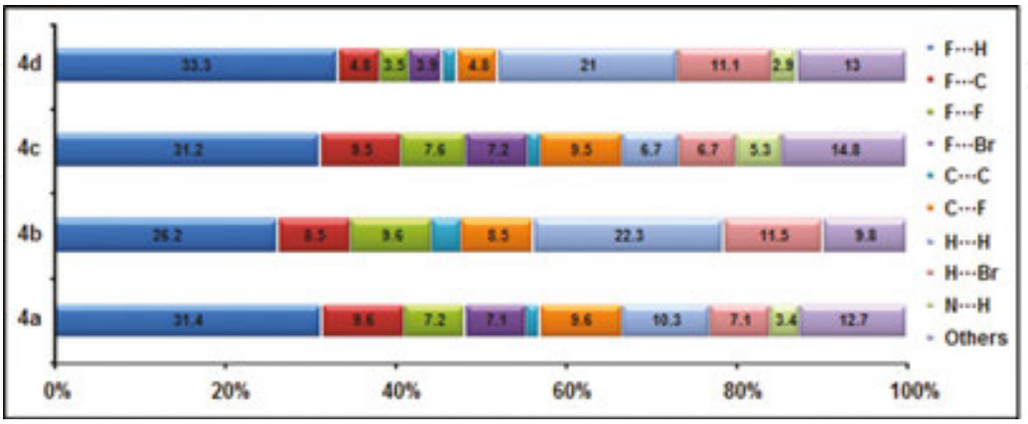


**Figure 14.** Percentage contribution of non-covalent interactions in porphyrins, **4a–4d** on the basis of HSs.

## 4. Conclusions

In conclusion, we have demonstrated the results of experimental crystallographic studies combined with computational HS analysis of a series of fluorinated porphyrins, **1–4**. The obtained results disclose that the isostructural couples exhibit similar kind of crystal packing in solid state with comparable intermolecular interactions. The HS analysis of compounds **1–4** indicates that the back bone of the net supramolecular arrangements are dictated by close contacts involving organic fluorine as well as C•••H and the cooperativity of weak H•••H interactions.

## Acknowledgements

SS (SR/WOS-A/CS-146/2011) and CA (SR/FT/CS-25/2011, SB/EMEQ-016/2013 and FRG 10-11/0103) thank DST, New Delhi and NIT Calicut for research funding. The authors thank the students of Bioinorganic Materials Chemistry Laboratory, Department of Chemistry, National Institute of Technology Calicut, namely Rahul Soman, Fasalu Rahman Kooriyaden and Ramesh J for their contributions. We would like to thank Dr. Shibu M. Eappen, STIC, CUSAT, Kochi and Dr. Babu Varghese, SAIF, IIT Madras for the single crystal data collection and structure solution, refinement respectively. The authors also thank Prof. T. N. Guru Row and Mr. Vijith kumar, Solid State and Structural Chemistry Unit, Indian Institute of Science, Bangalore for their help to get one of the single crystal X-ray data collections.

## Author details

Subramaniam Sujatha and Chellaiah Arunkumar*

*Address all correspondence to: arunkumarc@nitc.ac.in

Bioinorganic Materials Chemistry Laboratory, Department of Chemistry, National Institute of Technology Calicut, Kozhikode, Kerala, India

## References

[1] Hoard JL: In Smith KM, editor. Stereochemistry of Porphyrins and metalloporphyrins. New York: Elsevier; 1975, pp. 317–380.

[2] Rothemund P: A new porphyrin synthesis. The synthesis of porphin. J. Am. Chem. Soc. 1936;58:625–627. doi:10.1021/ja01295a027

[3] Adler AD, Longo FR, Kampas F, Kim J: On the preparation of metalloporphyrins. J. Inorg. Nucl. Chem. 1970;32:2443–2445. doi:10.1016/0022-1902(70)80535-8

[4] Adler AD, Longo FR, Finarelli JD, Goldmacher J, Assour J, Korsakoff L: A simplified synthesis for *meso*-tetraphenylporphin. J. Org. Chem. 1967;32:476. doi:10.1021/jo01288a053

[5] Lindsey JS, Wagner RW: Investigation of the synthesis of *ortho*-substituted tetraphenylporphyrins. J. Org. Chem. 1989;54:828–836. doi:10.1021/jo00265a021

[6] Lindsey JS, Schreiman IC, Hsu HC, Kearney PC, Marguerettaz AM: Rothemund and Adler–Longo reactions revisited. Synthesis of tetraphenylporphyrins under equilibrium conditions. J. Org. Chem. 1987;52:827–836. doi:10.1021/jo00381a022

[7] Maldotti A, Amadelli R, Bartocci C, Carassiti V, Polo E, Varani G: Photochemistry of Iron-porphyrin complexes. Biomimetics and catalysis. Coord. Chem. Rev. 1993;125:143–154. doi:10.1016/0010-8545(93)85014-U

[8] Chou JH, Kosal ME, Nalwa HS, Rakow NA, Suslick KS: Applications of porphyrins and metalloporphyrins to materials chemistry. Urbana: Academic Press; 2000.

[9] Sternberg ED, Dolphin D, Brickner C: Porphyrin-based photosensitizers for use in photodynamic therapy. Tetrahedron. 1998;54:4151–4202. doi:10.1016/S0040-4020(98)00015-5

[10] Rashid H, Umar MN, Khan K, Anjum MN, Yaseen M: Synthesis and relaxivity measurement of porphyrin-based magnetic resonance imaging (MRI) contrast agents. J. Struct. Chem. 2014;55:910–915. doi:10.1134%2FS0022476614050163

[11] Ethirajan M, Chen Y, Joshia P, Pandey RK: The role of porphyrin chemistry in tumor imaging and photodynamic therapy. Chem. Soc. Rev. 2011;40:340–362. doi:10.1039/B915149B

[12] Ojima I, editor. Fluorine in medicinal chemistry and chemical biology. UK: Wiley-Blackwell; 2009.

[13] DiMagno SG, Biffinger JC, Sun H: Fluorinated porphyrins and corroles: Synthesis, electrochemistry, and applications. Fluor. Heterocycl. Chem. 2014;1:589–620. doi: 10.1007/978-3-319-04346-3_14

[14] Berger R, Resnati G, Metrangolo P, Weberd E, Hulliger J: Organic fluorine compounds: A great opportunity for enhanced materials properties. Chem. Soc. Rev. 2011;40:3496–3508. doi:10.1039/C0CS00221F

[15] Desiraju GR. Crystal engineering: The design of organic solids. Amsterdam: Elsevier; 1989.

[16] Chopra D, Guru Row TN. Role of organic fluorine in crystal engineering. CrystEng-Comm. 2011;13:2175–2186. doi:10.1039/C0CE00538J

[17] Goldberg I. Crystal engineering of porphyrin framework solids. Chem. Commun. 2005;1243–1254. doi:10.1039/B416425C

[18] Spackman MA, Jayatilaka D. Hirshfeld surface analysis. CrystEngComm. 2009;11:19–32. doi:10.1039/B818330A

[19] Wolff SK, Grimwood DJ, McKinnon JJ, Turner MJ, Jayatilaka D, Spackman MA. Crystal Explorer 3.1 (2013), University of Western Australia, Crawley, Western Australia, 2005–2013. http://hirshfeldsurface.net/CrystalExplorer.

[20] McKinnon JJ, Mitchell AS, Spackman MA: Hirshfeld surfaces: A new tool for visualising and exploring molecular crystals. Chem. Eur. J. 1998;4:2136–2141. doi:10.1002/(SI-CI)1521-3765(19981102)4:11<2136::AID-CHEM2136>3.0.CO;2-G

[21] Spackman MA, McKinnon JJ: Fingerprinting intermolecular interactions in molecular crystals. CrystEngComm. 2002;4:378–392. doi:10.1039/b203191b

[22] Littler BJ, Ciringh Y, Lindsey JS: Investigation of conditions giving minimal scrambling in the synthesis of *trans*-porphyrins from dipyrromethanes and aldehydes. J. Org. Chem. 1999;64:2864–2872. doi:10.1021/jo982452o

[23] Adler AD, Longo FR, Kampas F, Kim J: On the preparation of metalloporphyrins. J. Inorg. Nucl. Chem. 1970;32:2443–2445. doi:10.1016/0022-1902(70)80535-8

[24] Altomare AG, Cascarano G, Giacovazzo C, Gualardi A: Completion and refinement of crystal structures with SIR92. J. Appl. Crystallogr. 1993;26:343–350. doi:10.1107/S0021889892010331

[25] Sheldrick GM. SHELXL97. Goettingen, Germany: University of Goettingen; 1997.

[26] Kadish KM, Araullo-McAdams C, Han BC, Franzen MM: Syntheses and spectroscopic characterization of (T(p-Me2N)F4PP)H2 and (T(p-Me2N)F4PP)M. J. Am. Chem. Soc. 1990;112:8364–8368. doi:10.1021/ja00179a021

[27] Schauer CK, Anderson OP, Eaton SS, Eaton GR: Crystal and molecular structure of a six-coordinate zinc porphyrin: Bis(tetrahydrofuran)(5,10,15,20-tetraphenylporphinato)zinc(II). Inorg. Chem. 1985;24:4082–4086. doi:10.1021/ic00218a024

[28] Tarahhomi A, Pourayoubi M, Golen JA, Zargaran P, Elahi B, Rheingold AL, Leyva Ramırezc MA, Percino TM: Hirshfeld surface analysis of new phosphoramidates. Acta Cryst. 2013;B69:260–270. doi:10.1107/S2052519213009445

[29] Bondi A: Van der Waals volumes and radii. J. Phys. Chem. 1964;68:441–451. doi:10.1021/j100785a001

[30] Batsanov SS: Van der Waals radii of elements. Inorg. Mater. 2001;37:871–885. doi:10.1023/A:1011625728803

[31] Grabowsky S, Dean PM, Skelton BW, Sobolev AN, Spackman MA, White AH: Crystal packing in the 2-R,4-oxo-[1,3-a/b]-naphthodioxanes–Hirshfeld surface analysis and melting point correlation. CrystEngComm. 2012;14:1083–1093. doi:10.1039/c2ce06393j

[32] Soman R, Sujatha S, Arunkumar C: Quantitative crystal structure analysis of fluorinated porphyrins. J. Fluor. Chem. 2014;163:16–22. doi:10.1016/j.jfluchem.2014.04.002

[33] Reed CA, Mashiko T, Scheidt WR, Spartalian K, Lang G: High spin iron (II) in the porphyrin plane. Structural characterization of (mesotetraphenylporphinato) bis (tetrahydrofuran)iron (II). J. Am. Chem. Soc. 1980;102:2302–2306. doi:10.1021/ja00527a028

[34] Schauer CK, Anderson OP, Eaton SS, Eaton GR: Crystal and molecular structure of a six-coordinate zinc porphyrin: Bis(tetrahydrofuran) (5,10,15,20- tetraphenylporphinato) zinc(II). Inorg. Chem. 1985;24:4082–4086. doi:10.1021/ic00218a024

[35] Bhyrappa P, Arunkumar C: Structural and electrochemical properties of β-tetrabromomesotetrakis(4-alkyloxyphenyl)porphyrins and their metal complexes. J. Chem. Sci. 2010;122:233–238. doi:10.1007/s12039-010-0027-6

[36] Bhyrappa P, Arunkumar C, Varghese B, Sankara Rao DS, Prasad SK: Synthesis and mesogenic properties of β-tetrabrominated tetraalkyloxyporphyrins. J. Porphyrins Phthalocyanines. 2008;12:54–64. doi:10.1142/S108842460800008X

[37] Scheidt WR: Systematics of the stereochemistry of porphyrins and metalloporphyrins, Kadish KM, Smith KM, Guilard R, New York: Academic Press; 2000, vol. 3, pp. 49–112.

[38] Kooriyaden FR, Sujatha S, Arunkumar C: Synthesis, spectral, structural and antimicrobial studies of fluorinated Porphyrins. Polyhedron. 2015;97:66–74. doi:10.1016/j.poly.2015.05.018

[39] Soman R, Sujatha S, De S, Rojisha VC, Parameswaran P, Varghese B, Arunkumar C: Intermolecular Interactions in fluorinated tetraarylporphyrins: An experimental and theoretical study. Eur. J. Inorg. Chem. 2014;2653–2662. doi:10.1002/ejic.201402008



IntechOpen